

Population I Wolf-Rayet Runaway Stars: the Case of WR124 and its Expanding Nebula M1–67

S.V. Marchenko¹, A.F.J. Moffat², P.A. Crowther³

ABSTRACT

In 1997 and 2008 we used the WFPC2 camera on board of the Hubble Space Telescope to obtain two sets of narrow-band H α images of the runaway Wolf-Rayet (WR) star WR 124 surrounded by its nebula M1–67. This two-epoch imaging provides an expansion parallax and thus a practically assumption-free geometric distance to the nebula, $d = 3.35 \pm 0.67$ kpc. Combined with the global velocity distribution in the ejected nebula, this confirms the extreme runaway status of WR 124. WR stars embedded within such ejection nebulae, at the point of core-collapse would produce different supernova characteristics from those expected for stars surrounded by wind-filled cavities. In galaxies with extremely low ambient metallicity, $Z \leq 10^{-3} Z_{\odot}$, γ -ray bursts originating from fast-moving runaway Wolf-Rayet stars may produce afterglows which appear to be coming from regions with a relatively homogeneous circumburst medium.

Subject headings: gamma-ray burst: general — stars: distances — stars: individual (WR 124) — stars: Wolf-Rayet — supernovae: general

1. INTRODUCTION

Among massive stars, those with the largest, continuous mass-loss rates are the Population I Wolf-Rayet (WR) stars. The impact of these fast, dense, clumpy and enriched winds on the ISM and stellar evolution itself cannot be overstated (e.g., Leitherer et al. 1992). The combination of high luminosity and sensitivity to initial relative heavy-element content

¹Science Systems and Applications, Inc., 10210 Greenbelt Road, Suite 600, Lanham, MD 20706, USA; sergey.marchenko@ssaihq.com

²Département de Physique and Observatoire du Mont Mégantic, Université de Montréal, CP 6128, Succursale Centre-Ville, Montréal, QC H3C 3J7, Canada; moffat@astro.umontreal.ca

³University of Sheffield, Department of Physics & Astronomy, Hicks Building, Hounsfield Rd, Sheffield, S3 7RH, UK; Paul.Crowther@sheffield.ac.uk

makes WR stars excellent tracers of the ambient metallicity gradients in star-forming galaxies. The WR stage is believed to precede supernova and hypernova explosions of type Ib/c (Crowther 2007), with a potential link to the long Gamma-Ray Bursts (GRB; e.g., Mirabal et al. 2003).

However, practically all distances to Galactic WR stars are notoriously uncertain. Any traditional distance estimates based on radial velocities of WR stars with subsequent application of the Galactic rotation law are always met with a good degree of skepticism: the optically thick, rapidly outmoving envelopes of WR stars distort any information about systemic motions of the stellar cores. Hence, modern distances are mainly based on spectroscopic parallaxes which, for an individual star, may appear to have relatively small errors, $\sim 30\%$ in the distance and perhaps even lower for WR stars in clusters/associations and in some binaries. However, these spectroscopic parallaxes are fraught with difficult-to-estimate systematic errors, making it essential to find other more direct techniques for distance determinations. With regard to the preferable, more robust astrometric approach: so far, only one parallax estimate has been made for the closest WR star, γ Vel (van der Hucht et al. 1997; revised by van Leeuwen 2007; the latter being supported by the interferometric measurements of North et al. 2007). All remaining WR stars have, so far, only lower limits to their parallax-based distances.

The situation is more appalling for the Galactic WN8 stars, i.e., for the spectral subclass of our target, WR 124 (209 BAC). Due to the tendency of WN8 stars to avoid clusters, associations and binary systems (see Marchenko et al. 1998 and references therein), one has to rely, almost exclusively, on spectroscopic parallaxes, thus introducing a large systematic uncertainty stemming from the necessarily simplified models of WR winds. One possible scenario to explain the apparently enigmatic characteristics of WN8 stars is that they are runaways, either ejected via slingshot-type dynamical interaction from the cores of forming dense star clusters (e.g., Evans et al. 2010), or accelerated by a SN explosion of the initial primary component in a binary system (De Donder et al. 1997). WR124 is of particular interest in this respect, given its large heliocentric radial-velocity (RV) component, $v = 137$ km s $^{-1}$, based on its associated nebular H α radial velocity (Sirianni et al 1998). As such, WR 124 is regarded to be among the fastest moving massive stars in the Galaxy (Moffat et al. 1982; see also the discussion in Moffat et al. 1998). The conclusion about the runaway status of WR 124 also heavily relies on the rather uncertain estimates of distance provided by (a) the fine structure components in the optical interstellar medium (ISM) lines seen towards WR 124 ($d \sim 4\text{--}5$ kpc: Crawford & Barlow 1991), and (b) the typical luminosities of similar-class WR stars in the Large Magellanic Cloud, leading to $d = 3.36$ kpc. Both estimates result in a high elevation of WR 124 above the Galactic plane, $z \geq 200$ pc, as compared to the average $|z| = 49$ pc for Galactic WR stars (van der Hucht 2001).

Firmly establishing the runaway nature of WR 124 may have an immediate impact on the problem of the environments of GRBs: in spite of the expectation of a $\sim r^{-2}$ density fall-off for a terminal-speed stellar wind, at least 1/5 of GRB afterglows indicate a constant-density medium around the exploding star (van Marle et al. 2006; Starling et al. 2008). An extremely rapid motion ($\sim 100 \text{ km s}^{-1}$) of a WR progenitor should lead, on an evolutionary timescale, to a displacement of the WR star from its place of birth (usually, a star-forming region), as well as from the center of a bubble blown by the predecessor’s wind, i.e. deep into the surrounding and, presumably, more uniform ISM. This is in line with the findings of Hammer et al. (2006) that some long GRBs may occur several hundred parsecs outside of the rich and compact clusters or star-forming regions whence they presumably originated, thus defying the *general* tendency of GRBs to concentrate on the brightest regions of their host galaxies (Svensson et al. 2010). Considering the possible link of WR stars and, in particular, WR runaways to GRBs, one should also be aware that WN8 stars belong to the late-type WN (WNL) subgroup, which comprises the most massive and luminous Population I WR stars. Moreover, while there is considerable variation in hydrogen content from one WN8 star to another, some WN8 stars are practically devoid of hydrogen (see Marchenko et al. 1998 and references therein). Note that WR 124 is further sub-classified as WN8h and so contains a non-negligible amount of atmospheric hydrogen (Crowther et al. 1999, C99).

There is an additional aspect which makes WR 124 an attractive target for a detailed study. More than 1/4 of all WR stars are currently surrounded by detectable nebular shells, seen projected in the form of ring-like structures, i.e. “ring nebulae” (RNe; Chu et al. 1983, Marston et al. 1994). All WR stars have likely possessed a RN at some stage in their evolution (Dopita et al. 1994). RNe are believed to be formed via the interaction between a slow wind of the predecessor and a fast wind associated with the presently observed Population I WR star (e.g. Marston 1995). Our target belongs to the RN group. The surrounding nebula, M 1–67, is a relatively young ejection-type, low-excitation nebula (Chu et al. 1983; Smith 1995), probably in the earliest [so far] observed phase of wind interaction around any Population I WR star. This is compatible with the relatively high H abundance of the central star. The narrow-band net H α image of M1–67 acquired with HST/WFPC2 in 1997 (Grosdidier et al., 1998) showed a wealth of complex details, some of which have never been seen before in such a nebula. In an attempt to derive a relatively assumption-free distance to WR 124/M1–67 based on nebular expansion, we obtained a second-epoch image of the nebula in 2008.

2. OBSERVATIONS AND DATA REDUCTION

On March 16, 1997, the HST/WFPC2 camera was used to secure a net- $H\alpha$ (F656N) image of M1–67 (Grosdidier et al., 1998, 2001). The combination of four 2500 sec exposures provided a deep, high signal-to-noise Epoch-1 (E1) image. The Epoch-2 (E2) HST/WFPC2 image was constructed from 8 500-600 sec-long exposures in $H\alpha$ (F656N) obtained on June 21, 2008 in the 4-point dither pattern with the cosmic-ray split option. The chosen total exposure time, though substantially shorter than in the E1 imaging, nevertheless assured adequately high S/N ratios for all parts of the nebula, in addition to reducing the impact of the saturated regions surrounding the central star.

All the 1997 and 2008 images were processed using standard IRAF¹ utilities, in particular the *stdas/analysis/dither* subroutines. The relative orientation of the E1 and E2 images, with the latter rotated by ~ 90 degrees due to the technical limitations posed by the 2-gyro guidance mode, prevented a straightforward, camera-to-camera comparison of the images. For inter-comparison of E1 and E2 we chose 5 regions well distributed azimuthally around the central star, where the presence of strong, sharp features allowed the best determination of the nebular expansion rate. Three of them are sampled by the W3 camera: in one case the central star and its immediate surroundings are imaged by W3 in E1 and E2 (Fig. 1); in the second case the overlapping regions are imaged by W2 in E1 and W3 in E2; the third case combines W3 from E1 and W4 from E2. In the two remaining cases we combine the overlapping regions in W4 from E1 and PC from E2, then PC from E1 and W2 from E2. All of the chosen cases depict sufficiently bright parts of the nebula and an adequate number of background/foreground stars which may be used for a fine co-alignment of the E1 and E2 images. Choosing the appropriate regions, one also has to find a compromise between the two conflicting factors: opting for remote regions of the nebula, one may minimize the bias introduced by infrequent plane-of-the-sky projections; on the other hand, the velocity fields of the remote regions may be distorted by the bow-shock interface surrounding the nebula (van der Sluys & Lamers 2003).

All the available images were cleaned of cosmic rays, corrected for camera distortions, then iteratively shifted and rotated using a combination of the cross-correlation technique (e.g., *crossdriz*) and the reference-star approach (e.g., *imcentroid*). In two cases we magnified the Planetary Camera images by adjusting their pixel scales which were derived by measuring distances between multiple reference stars. Finally, the relative shifts between out-moving

¹IRAF is distributed by the National Optical Astronomy Observatory, which is operated by the Association of Universities for Research in Astronomy, Inc. under cooperative agreement with the National Science Foundation.

parts of the nebula were estimated by choosing small ($\sim 100 \times 100$ pixels) sections of the overlapping E1 and E2 images with the most obvious relative shifts and allowing the E1 sub-raster to move in x, y directions with 0.01-pixel increments. Such gradual, small-scale shifts, at some point, should minimize the difference (assessed via standard deviation; see Fig. 1 for examples of the differences) between the E1 and E2 sub-rasters, thus providing an estimate of the radial expansion rate.

3. RESULTS AND CONCLUSIONS

Long-slit spectroscopy of M1–67 established that the bulk of the nebula expands at $v_{\text{exp}}=42\text{--}46 \text{ km s}^{-1}$ (Solf & Carsenty 1982; Sirianni et al. 1998). In our calculations we adopt the latter value ($v_{\text{exp}}= 46 \text{ km s}^{-1}$) which is based on a comprehensive modelling of the nebular expansion. All 5 measurements (Fig 2) point to a fairly uniform expansion between E1 and E2 ($\Delta t = 11.26 \text{ yr}$) of $\Delta r = 0.326 \pm 0.059$ pixels, or $\Delta r = 0.''0326 \pm 0.''0059$. Assuming these expansions to be essentially radial, this translates into a distance to M1–67 of $d = 3.35 \pm 0.67 \text{ kpc}$, in perfect (although fortuitous) accord with the estimate from van der Hucht (2001), under the assumption of $M_v = -5.5 \text{ mag}$ for the central star. The 20% distance error comes from the combination of the $\sim 10\%$ uncertainty in the expansion velocity of the nebula and the above-mentioned 18% error of the geometric expansion. The latter corresponds to the standard deviation of the sample of 5 independent measurements. We prefer this straightforward and, potentially, less biased estimate over the formal error analysis of the x, y components of the expansion patterns in the individual regions. The x, y errors would depend on, most of all, the detailed morphology of a given region, as well as different S/N ratios of the region’s fine structures, which may lead to unaccountable biases. Though we selected the relatively remote regions of M1–67 (Fig 2), there is always a chance that *all* of them have been affected by the plane-of-the-sky projection effect. One may not completely disregard this possibility. However, considering the tight clustering of the derived expansions (0.368,0.367,0.334,0.338,0.224 pixels), we conclude that 4 out of 5 randomly selected regions may have orientations fairly close to the plane-of-the-sky.

Such a distance unequivocally assigns a runaway status to WR124. Indeed, the star is moving fast, judging by the high peculiar $RV \sim 156 \text{ km}^{-1}$ of the star and its surrounding nebula (Moffat et al 1982). Given $b = +03.31^\circ$, $d = 3.35 \text{ kpc}$ leads to an elevation of $z = 193 \pm 39 \text{ pc}$ above the Galactic plane, or 4 times the average $|z| = 49 \text{ pc}$ for Galactic Population I WR stars. Nothing significant can be said about the tangential (proper) motion of WR124, since the Hipparcos data are insufficiently accurate for such distant stars (Moffat et al. 1998). The $d = 3.35 \text{ kpc}$ distance implies a physical radius of 0.9 pc for M1–67 based

on its $55''$ radius (Solf & Carsenty 1982; Grosdidier et al. 1998), and so a dynamical age of 21,000 yr for our adopted 46 km^{-1} expansion rate.

On the basis of the geometric distance to WR 124/M1-67, we have re-derived the physical properties of WR 124 using ultraviolet, optical and near-infrared spectroscopic datasets from C99 plus the model atmosphere code CMFGEN (Hillier & Miller 1998). Our analysis mimics C99, except that line blanketing by additional elements is incorporated, namely oxygen, neon, sulfur, argon, calcium and nickel, such that, in total, a factor of three more spectral lines are considered. A slightly higher stellar temperature of 36 kK is obtained, while the reduced distance with respect to that adopted by C99 (5 kpc) yields a lower luminosity and mass-loss rate for identical adopted clumping factors of $f = 0.1$, with an atmospheric hydrogen content ($\sim 15\%$ by mass) unchanged. We compare the newly derived properties of WR124 with C99 and Hamann et al. (2006, H06) in Table 1. Stellar masses are estimated in each case using the mass-luminosity relation for hydrogen-free WR stars of Schaerer & Maeder (1992). We have compared our results with contemporary evolutionary models for single stars at solar composition (Meynet & Maeder 2003). The closest agreement is found for an initially rotating $25 M_{\odot}$ model after 8.6 Myr, although this remains somewhat more luminous and hydrogen-rich than WR 124, with $\log L/L_{\odot}=5.47$ and $\text{H/He}=1.5$ ($X_{\text{H}} = 27\%$).

Our target is unlikely to undergo a GRB since such events are predominantly found in faint, metal-poor host galaxies (e.g. Modjaz et al. 2008). Nevertheless, the proven runaway status of a Population I WR star may provide some insights for interpretation of the afterglows coming from a specific category of GRBs. Let us assume that a rapidly moving massive star produces a long GRB. The circumburst media are usually probed by modeling the temporal decay of afterglows (Chevalier & Li 2000), with preference given to the late (0.1 day and more) phases of an afterglow, in order to lessen the impact of any prompt-emission components. As a consequence, typical time-spans used in the recent models of afterglows cluster around 10^5 sec (e.g., Starling et al 2008). Hence, if an afterglow points to a seemingly homogeneous environment in the *immediate* surroundings of the burst, the size of the wind-filled cavity should not exceed a few light-days. Otherwise, in an unbound, freely expanding stellar wind the density profile would fall off proportionally to r^{-2} . In the case of WR 124 the density of the ejected M1-67 nebula falls off as $r^{-0.8}$ (Grosdidier et al. 1998). Considering the high RV of the ejecta, one may assume that the nebula was created when the star already gained high spatial velocity. Hence, the nebula, most likely, travels along with the central star. However, the star’s immediate surroundings (out to at least light-weeks: the star has been known as a WR for more than 50 years) are filled by a fast

Table 1. Comparison between physical and wind properties of WR124 (WN8) derived by Crowther et al. (1999, C99), Hamann et al. (2006, H06) and the present study.

Study	C99	H06	This study
T_* (kK)	32.7	44.7	35.8 ± 2
R_* (R_\odot)	18.0	16.7	$10.1^{+2.8}_{-2.6}$
$\log L/L_\odot$	5.53	6.0	$5.18^{+0.2}_{-0.24}$
M/M_\odot	14:	33:	9 ± 2.5
v_∞ (km s^{-1})	710	710	710
f	0.1	0.25	0.1
\dot{M} ($M_\odot \text{ yr}^{-1}$)	$10^{-4.7}$	$10^{-4.1}$	$10^{-4.95 \pm 0.15}$
H/He (X_{H})	0.7 (15%)	0.6 (13%)	0.75 ± 0.1 (15±2%)
m_v (mag)	11.58	11.58	11.58
A_v (mag)	4.4:	4.1	4.3 ± 0.1
d (kpc)	5	8.4	3.35 ± 0.67
M_v (mag)	-6.3	-7.2	$-5.3^{+0.4}_{-0.5}$

Note. — Stellar mass estimates are obtained from the mass-luminosity relation for hydrogen-free WR stars (Schaerer & Maeder 1992).

stellar wind. This would result in a clear ‘wind-imprinted’ afterglow after a hypothetical GRB. Therefore where do the \sim constant-density profiles come from?

A massive runaway star with a strong wind, moving through the ISM at supersonic velocity creates a leading bow shock (e.g., Vela X-1: Kaper et al. 1997). Beyond the wind-filled cavity and the bordering bow-shock, both occurring relatively close to the central star, one may expect to see an unperturbed, ‘homogeneous’ interstellar environment. The bow-shock stand-off distance, d_s , can be expressed as (Huthoff & Kaper 2002):

$$d_s = \frac{0.9pc}{(v_\star/50km\ s^{-1})} \sqrt{\frac{(\dot{M}/10^{-6}M_\odot) \times (v_\infty/10^3km\ s^{-1})}{(n/cm^{-3})}}$$

where \dot{M} is the mass-loss rate and v_∞ is the terminal wind velocity.

The peculiar spatial velocity of WR 124 may reach $v_\star \sim 200\ km\ s^{-1}$ (e.g. Moffat et al 1982). However, the typical [high] mass-loss rate of a Galactic WN8 star prevents d_s from dropping much below a few light-months, instead of the required light-days. Indeed, van der Slyus and Lamers (2003) find that M1–67 is confined by a bow shock with [model-dependent] $d_s = 1.3\ pc$. The situation changes dramatically once we invoke the fact that the long GRBs preferentially occur in low-metallicity environments. In this case one must take into account the dependence of the mass-loss rate and the terminal velocity of the wind on the metallicity of the host galaxy: $\dot{M} \sim Z^{0.83}$ (Mokiem et al. 2007), and $v_\infty \sim Z^{0.13}$ (Leitherer et al. 1992). In addition, the rest-frame spatial interstellar densities, n , of the regions hosting GRBs usually exceed the corresponding densities in the disk of the Milky Way Galaxy by 1-2 orders of magnitude (Nardini et al. 2010). A typical WN8 wind with $\dot{M} \sim 5 \times 10^{-6} M_\odot yr^{-1}$ and $v_\infty \sim 10^3\ km\ s^{-1}$ (Hamann et al. 2006), once appropriately scaled down for a $Z = 10^{-3} Z_\odot$ environment to $\dot{M} \sim 1.6 \times 10^{-8} M_\odot yr^{-1}$ and $v_\infty \sim 400\ km\ s^{-1}$, would create a rather small wind-blown cavity around a fast-moving star with d_s of the order of a few light-days. This should increase the chance of at least one of the ensuing GRB jets to promptly leave the wind-filled cavity and induce an afterglow which could be perceived as coming from an approximately constant-density environment unperturbed by a stellar wind.

WR 124 itself is not likely to end its life as a GRB. However, it may explode as a core-collapse SN, either a Type IIb or Ib. Both flavours of core-collapse SNe are closely associated with star-forming regions and agglomerates of massive stars (Smartt 2009). The possible association of a dense ejection nebula, such as M1–67, with the immediate supernova progenitor also has relevance to the interpretation of the interaction between the SN blastwave and the inner circumstellar material (Chevalier 1982), as, for example, measured by radio observations (Weiler et al. 2002).

Pondering the origin of the high spatial velocity of WR 124, we note that the star

moves away almost radially (van der Sluys & Lamers 2003). The absence of any rich cluster/association in the star’s vicinity, as well as the relatively low initial stellar mass (the newly derived luminosity suggests the current mass of $\sim 9 M_{\odot}$) point to a modest parent cluster, if any. However, the high RV of the star calls for strong dynamical interactions in a dense core of a rich stellar cluster, contrary to observations. Hence, it seems more likely that WR 124 has gained the runaway status following the recoil after a SN explosion in a close binary system.

We conclude that the relatively assumption-free, geometric distance to WR 124 reinforces the runaway status of the star. The implied high peculiar velocity should result in a large displacement of WR 124 from its place of origin, thus potentially moving the runaway into a region with relatively unperturbed ISM. The latter may help to explain the occurrence of a substantial fraction of GRB afterglows in regions with a seemingly constant-density circumburst medium, contrary to the expectations of a $\sim r^{-2}$ density fall-off for a typical massive-star wind. However, an appropriately small (\sim light-day) wind-filled cavity may only be formed by a massive runaway star born in a low-metallicity environment, $Z \leq 10^{-3} Z_{\odot}$: cf. $Z = 10^{-2} Z_{\odot}$ for the host of GRB 050730 (Chen et al. 2005). Hence, this particular category of GRB may emerge exclusively from regions with a *very* low metallicity content, thus conforming to the general conclusion of Han et al. (2010) that long GRBs should occur in a relatively pristine ISM.

This study was based on observations made with the NASA/ESA Hubble Space Telescope and obtained from STScI, which is operated by AURA Inc., under NASA contract NAS 5-26555. Support for Program number GO11137 was provided by NASA through a grant from the STScI, which is operated by AURA Inc., under NASA contract NAS 5-26555. AFJM is grateful for financial assistance to NSERC (Canada) and FQRNT (Québec).

REFERENCES

- Chevalier, R.A. 1982, ApJ, 258, 790
- Chevalier, R.A., & Li, Z.-Y. 2000, ApJ, 536, 195
- Chen, H.-W., et al., 2005, ApJ, 634, L25
- Chu, Y.-H., et al. 1983, ApJS, 53, 937
- Crawford, I.A., & Barlow, M.J. 1991, A&A, 249, 518

- Crowther, P.A. 2007, *ARA&A* 45, 177
- Crowther, P.A. et al. 1999, *A&A*, 350, 1007 (C99)
- De Donder, E., Vanbeveren, D., & van Bever, J. 1997, *A&A*, 318, 812
- Dopita, M.A., et al. 1994, *ApJS*, 93, 455
- Evans, C.J., et al. 2010, *ApJ*, 715, L74
- Grosdidier, Y., et al. 2001, *ApJ*, 562, 753
- Grosdidier, Y., Moffat, A.F.J., Joncas, G., & Acker, A. 1998, *ApJ*, 506, L127
- Hamann, W.-R., Gräfener, G., & Liermann, A. 2006, *A&A*, 457, 1015
- Hammer, F., et al. 2006, *A&A*, 454, 103
- Han, X.H., et al. 2010, *A&A*, 514, 24
- Hillier, D.J., & Miller, D.L. 1998, *ApJ*, 496, 407
- Huthoff, F. & Kaper, L. 2002, *A&A*, 383, 999
- Kaper, L., et al. 1997, *ApJ*, 475, L37
- Leitherer, C., Robert, C., & Drissen, L. 1992, *ApJ*, 401, 596
- Marchenko, S., et al. 1998, *MNRAS*, 294, 642
- Marston, A.P. 1995, *AJ*, 109, 1839
- Marston, A.P., et al. 1994, *ApJS*, 93, 229
- Meynet G., & Maeder A. 2003, *A&A* 404, 975
- Mirabal, N., et al. 2003, *ApJ*, 595, 935
- Modjaz, M. et al. 2008, *AJ*, 135, 1136
- Moffat, A.F.J., Lamontagne, R., & Seggewiss, W. 1982, *A&A*, 114, 135
- Moffat, A.F.J., et al. 1998, *A&A*, 331, 949
- Mokiem, M.R., et al. 2007, *A&A*, 473, 603
- Nardini, M., Ghisellini, G., Ghirlanda, G., & Celotti, A. 2010, *MNRAS*, 403, 1131

- North, J.R., et al. 2007, MNRAS, 377, 415
- Schaerer, D., & Maeder A. 1992, A&A, 263, 129
- Smartt, S.J. 2009, ARA&A, 47, 63
- Smith, L.J. 1995, in IAU Symp. 163, p. 24
- Sirianni, M., Nota, A., Pasquali, A., & Clampin, M. 1998, A&A, 335, 1029
- Solf, J., Carsenty, U. 1982, A&A, 116, 54
- Starling, R.L.C., et al. 2008, ApJ, 672, 433
- Svensson, K.M., et al. 2010, MNRAS, 405, 57
- van der Hucht, K.A. 2001, New Astron. Rev., 45, 135
- van der Hucht, K.A., et al. 1997, New Astronomy, 2, 245
- van der Sluys, M.V., & Lamers, H.J.G.L.M. 2003, A&A, 398, 181
- van Leeuwen, F. 2007, Hipparcos, the New Reduction of the Raw Data, (Dordrecht: Springer)
- van Marle, A.J., Langer, N., Achterberg, A., & García-Segura, G. 2006, A&A, 460, 105
- Weiler, K.W., Panagia, N., Montes, M.J. & Sramek, R.A. 2002, ARA&A 40, 387

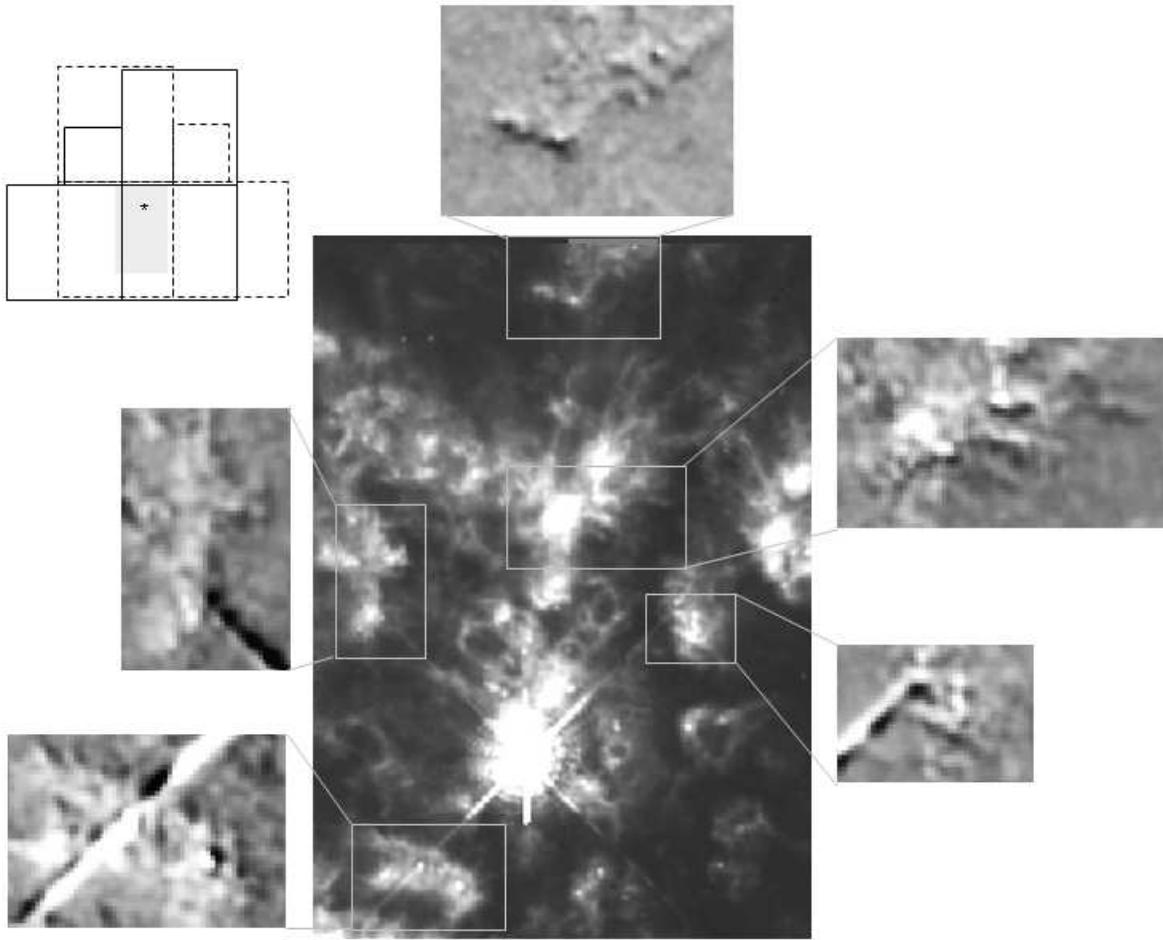


Fig. 1.— The sketch in the upper-left corner shows the orientation of the E1 (full lines separating the W2,W3,W4 and PC devices) and E2 (dashed lines) HST images taken with the 656N filter. The central star is placed in W3 for both epochs. The shaded area in the sketch corresponds to the part of the W3 (E2) image shown in the main section of the figure. The magnified parts of the W3 image show the E2-E1 differences, where the proper motions are most easily detected via relatively strong, sharp nebular edges.

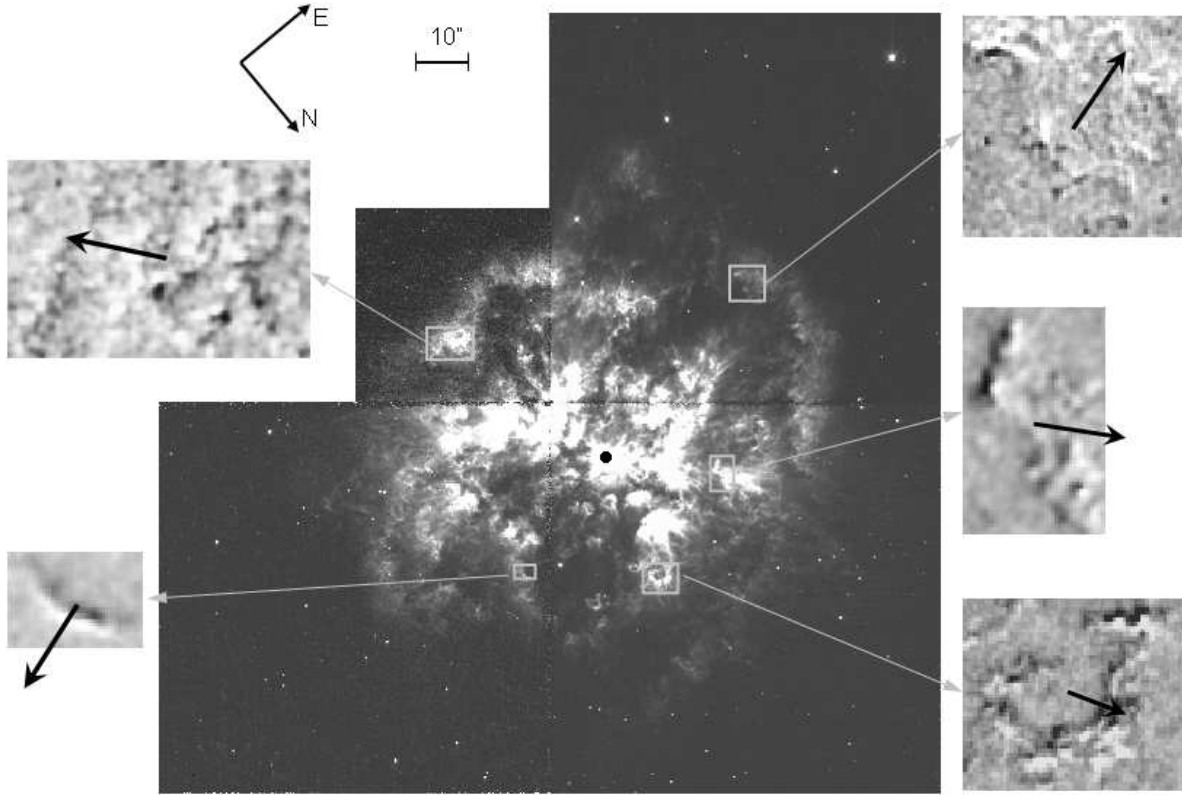


Fig. 2.— The E2 656N image of M1-67 with the central star marked by a dot. The enlarged areas show the E2-E1 difference images used to estimate the geometric expansion of the nebula. The direction and size of the black arrows depict the measured proper motions of the corresponding parts of the nebula. The scale and orientation of the image are provided in the upper left corner.